Supporting information

A bioinspired magnetically driven mother–child robot with controllable exfoliation behavior for targeted drug delivery

Dingwen Tong[2,6], Xinjian Fan[1,6], Yanshuo Wei[1], Xuanyi Huang[3], Yinglun Zhou[3], Jinghan Gao[3], Shangnong Dong[3], Hui Xie[5], Jiajing Su[3], Wanning Ge[1], Yanlei Hu*[2,4] and Zhan Yang*[1]*

[1] School of Mechanical and Electrical Engineering, Soochow University, Suzhou 215000, China.

[2]CAS Key Laboratory of Mechanical Behavior and Design of Materials, Department of Precision Machinery and Precision Instrumentation, University of Science and Technology of China, Hefei 230027, China.

[3]School of Future Science and Engineering, Soochow University, Suzhou 215222, China.

[4]Department of Obstetrics and Gynecology, The First Affiliated Hospital of USTC, Division of Life Sciences and Medicine, University of Science and Technology of China, Hefei, 230001, China.

[5]School of Mechatronics Engineering, Harbin Institute of Technology, Harbin, 150001, China.

[6]These authors contributed equally: Dingwen Tong, Xinjian Fan.

E-mail: xinjianfan@suda.edu.cn; huyl@ustc.edu.cn; yangzhan@suda.edu.cn.

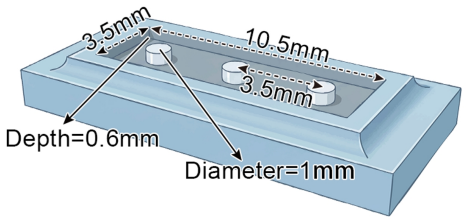

Fig. S1 Mold dimensions for preparing the MR magnetic soft framework.

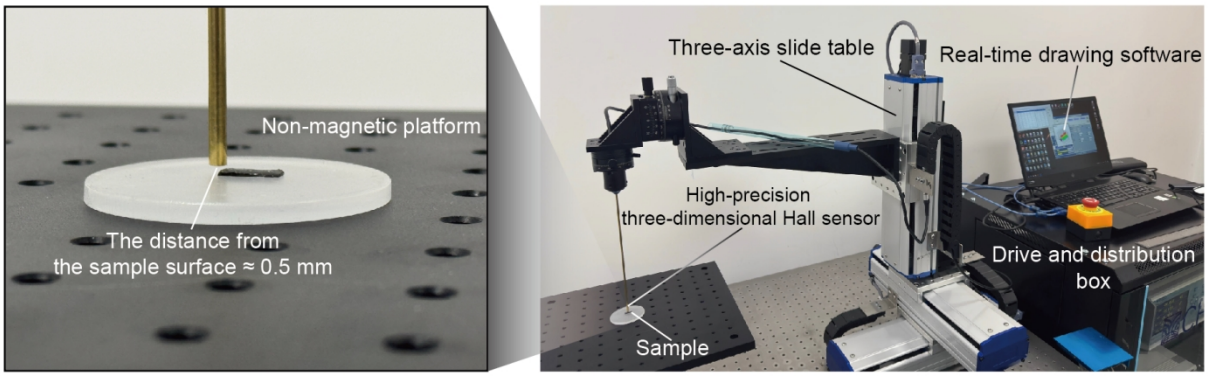

Fig. S2 Composition of the MR surface magnetic moment measurement system. During the measurement process, it was carried out on an aluminum non-magnetic platform. The distance between the end of the high-precision three-dimensional Hall sensor and the upper surface of the MR is 0.5mm.

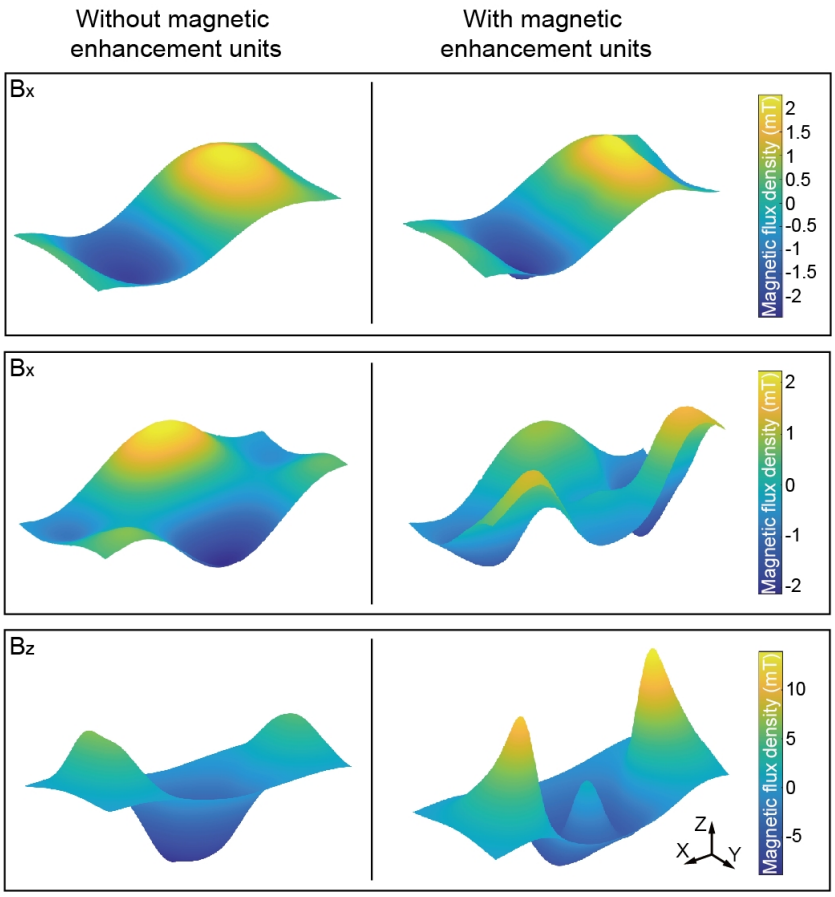

Fig.S3 MR surface magnetic moment in the x, y, and z directions. Among them, the distribution of B_z is highly similar to the spatial distribution of the total magnetic moment B.

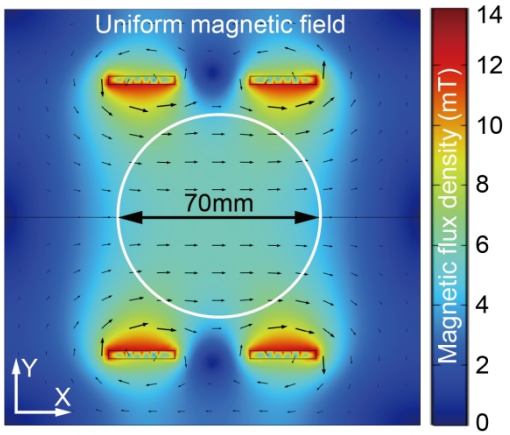

Fig. S4 Simulation results of a uniaxial Helmholtz coil generating a uniform magnetic field.

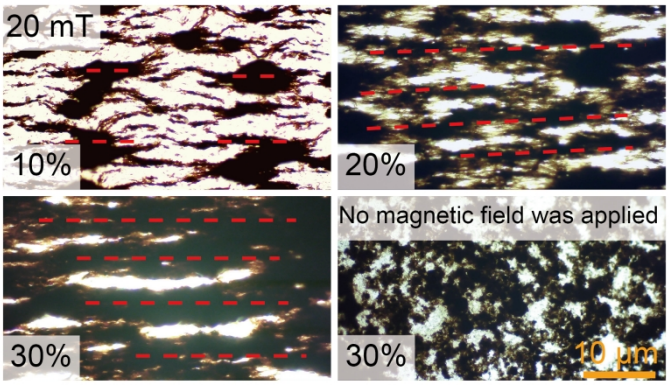

Fig. S5 Optical micrographs of Fe_3O_4 chains formed in gelatin at different mass fractions. Fe_3O_4-based gelatin solutions with Fe_3O_4 particle mass fractions of 10%, 20%, and 30% were dropped onto hot slides soaked in 40°C water, and the slides were placed in a 20 mT magnetic field. Then, cover slips frozen in the refrigerator were used to cover the liquid to form a solidified thin-layer sample, and the sample could then be observed under an optical microscope. Samples without applying a magnetic field during the solution solidification process were prepared using the same method. These samples did not form microscopic chain-like structures.

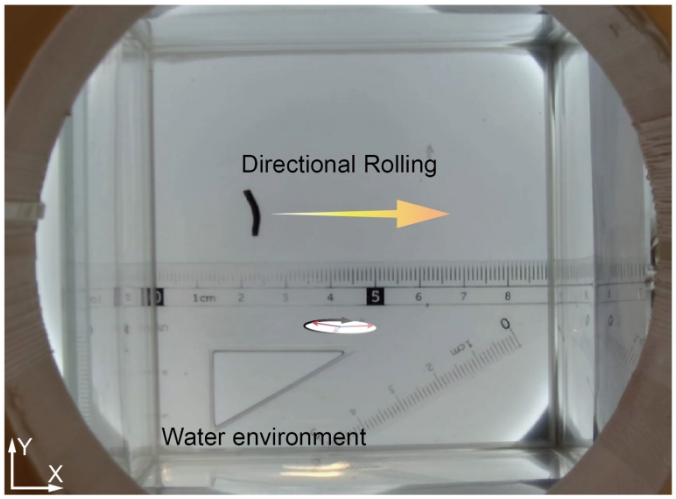

Fig. S6 Experimental environment for evaluating the movement speed and phenomena of MR under different magnetic field conditions, with the bottom inclination angle set to 0°.

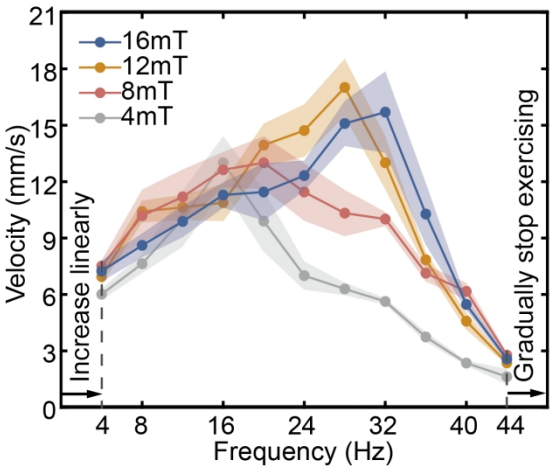

Fig. S7 The movement speed of CR within the horizontal plane under different magnetic field conditions. Similar to MR, CR shows a trend of increasing speed first and then decreasing as the frequency of the rotating magnetic field increases. However, under the same conditions, its movement speed is slower than that of MR.

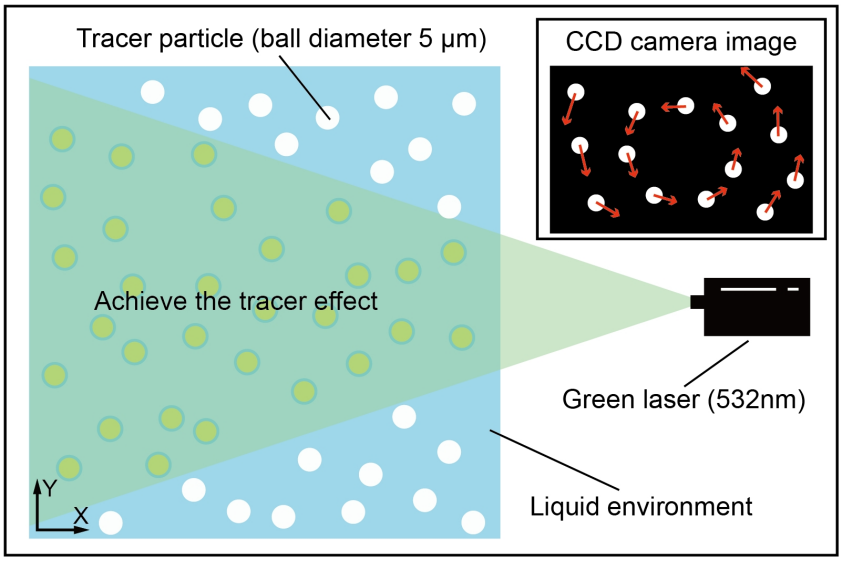

Fig. S8 The principle of PIV flow field reconstruction.

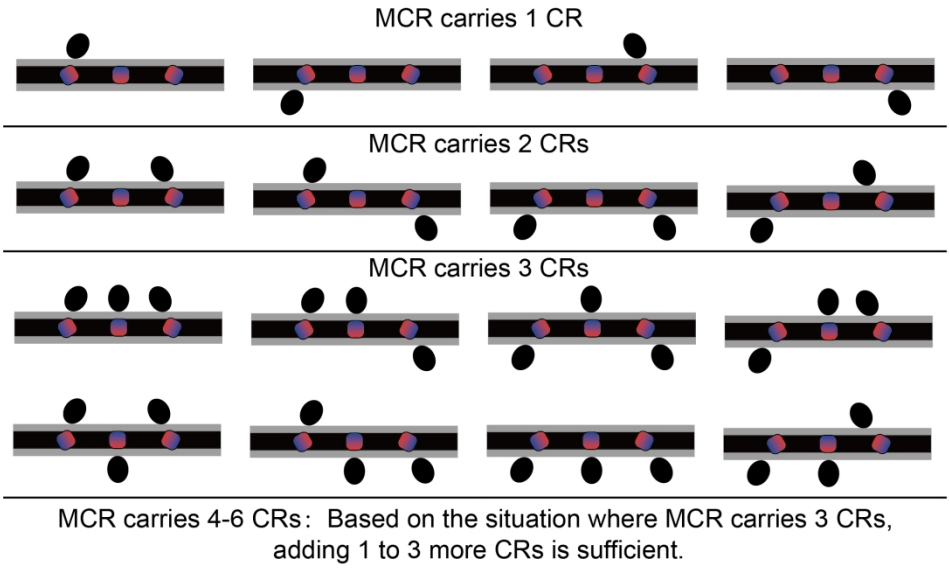

Fig. S9 In the experiment to test the conditions for the detachment of CRs, various scenarios where MR carries different numbers of CRs

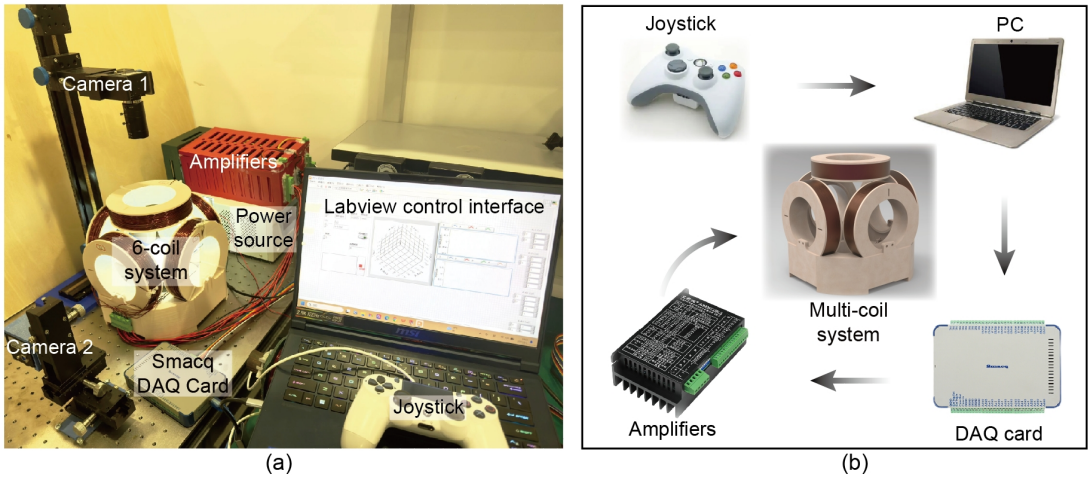

Fig. S10 The composition of the magnetic control system and the process of control signal transmission. (a) The hardware composition of the 6-coil system, where the robot's position within the working space is observed by two industrial cameras in the horizontal and vertical directions. (b) The flow direction of the control signals, where the joystick transmits the information of the expected magnetic field to the PC, and the LabVIEW program on the PC calculates the control signals and outputs them to the DAQ card. The DAQ card then sends analog signals to different amplifiers, which increase the output voltage and current capacity of the amplifiers. Finally, the output ends of different amplifiers are connected to the corresponding coil units.

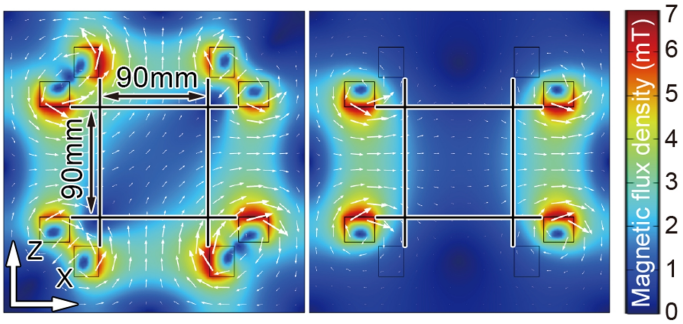

Fig. S11 The simulation results of the approximately uniform rotating magnetic field generated by the six-coil system.

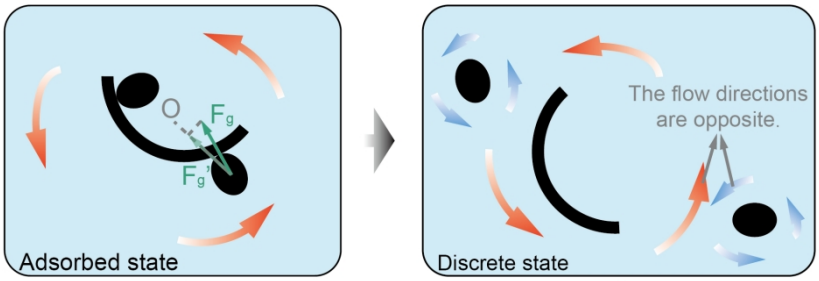

Fig. S12 The force conditions during the detachment process of CRs from MR. (a) Schematic diagram of the principle when CRs are detached from MR. As the overall rotational speed of MCR increases, when the attractive force of MR on CRs cannot meet the requirement of the required centripetal force, CRs will detach from MR. (b) Schematic diagram of the principle of the repulsion generated after CRs detach from MR. Since the detached CRs will also spin in the horizontal rotating magnetic field, when CRs and MR come close again, the flow velocity direction at the intersection point of the flow field is opposite, resulting in a repulsive effect.

Movie S1. The preparation details and characterization results of CR.

- The process of titrating the Fe3O4-based gel solution into the liquid paraffin at low temperature.
- When the environmental magnetic field intensity and the content of Fe3O4 are different, the morphology of CR is obtained.
- The temperature changes during the titration of the high-temperature Fe3O4-based gel solution to liquid paraffin at 0°C.
- Infrared thermal imaging of the CR process of high-frequency solenoid magnetic hysteresis heating.
- Infrared thermal imaging of the CR process during NIR near-infrared laser irradiation.

Movie S2. The specific trajectory movement of MCR and its adaptability to various terrains.

- MCR smoothly proceeds along the "M", "C" and "R" trajectories respectively.
- Floating across the ditch.
- Passing through the multiple crevices.
- Climbing over the protruding peak.
- Ascending across the water-land interface.

Movie S3. The adsorption and desorption behaviors of CR as well as the effect of PIV flow field reconstruction.

- The process of CR being adsorbed and stripped off.
- PIV flow field reconstruction during the CR spiral motion process.
- PIV flow field reconstruction during the process of CR separation.

Movie S4. Ultrasonic tracing of MCR and gastric drug delivery.

- Ultrasound tracking of MCR's rolling movement in the excised porcine stomach.
- MCR's dual-target drug delivery in the excised porcine stomach.

Movie S5. The Process of Quick and Slow Drug Release.

- Quick release.
- Slow release.

Movie S6. Magnetic drive system's magnetic field simulation.

- Magnetic field simulation of the six-coil system.
- Magnetic field simulation of the eight-coil system.